Article

Molecular Cell

Msp1 Is a Membrane Protein Dislocase for Tail-Anchored Proteins

Graphical Abstract

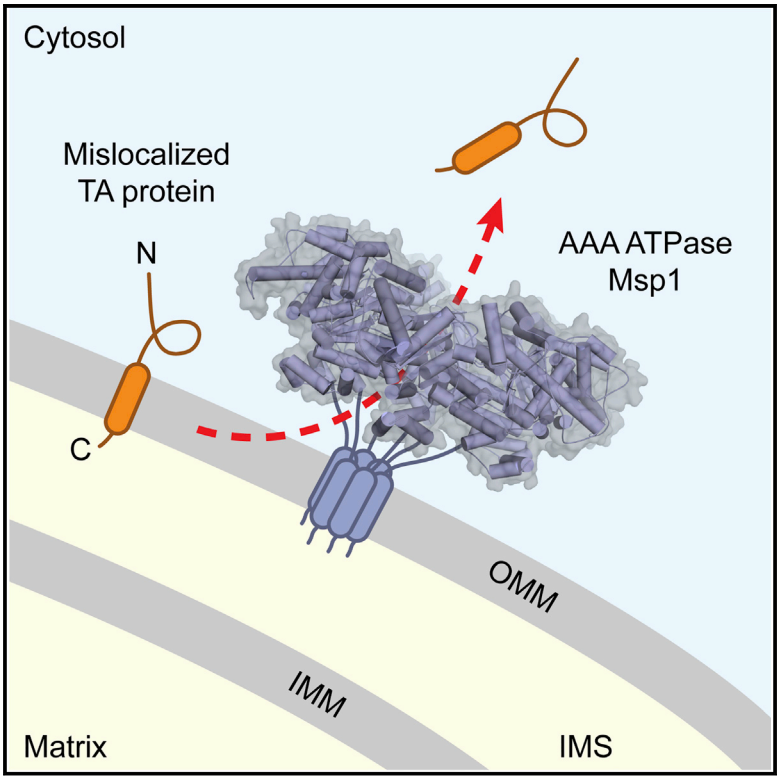

Authors

Matthew L. Wohlever, Agnieszka Mateja, Philip T. McGilvray, Kasey J. Day, Robert J. Keenan

Correspondence

bkeenan@uchicago.edu

In Brief

The AAA ATPase Msp1 plays a central role in clearing mislocalized tail-anchored proteins from the outer mitochondrial membrane. Wohlever et al. use a purified, reconstituted system and structural analysis to show that Msp1 is necessary and sufficient for the ATP-dependent extraction of fully integrated TA proteins from the bilayer.

Highlights

- Msp1 is necessary and sufficient to dislocate TA proteins from membranes
- The AAA domain of Msp1 forms ATP-dependent hexamers in solution
- Conserved residues in the central pore of Msp1 are essential for TA protein extraction
- Heterologous TMD sequences can functionally substitute for the Msp1 TMD

Wohlever et al., 2017, Molecular Cell 67, 194–202
July 20, 2017
http://dx.doi.org/10.1016/j.molcel.2017.06.019

CellPress

Molecular Cell
Article

Msp1 Is a Membrane Protein Dislocase for Tail-Anchored Proteins

Matthew L. Wohlever,[1] Agnieszka Mateja,[1] Philip T. McGilvray,[1] Kasey J. Day,[2] and Robert J. Keenan[1,3,*]
[1]Department of Biochemistry and Molecular Biology, The University of Chicago, 929 East 57th Street, Chicago, IL 60637, USA
[2]Department of Molecular Genetics and Cell Biology, The University of Chicago, 920 East 58th Street, Chicago, IL 60637, USA
[3]Lead Contact
*Correspondence: bkeenan@uchicago.edu
http://dx.doi.org/10.1016/j.molcel.2017.06.019

SUMMARY

Mislocalized tail-anchored (TA) proteins of the outer mitochondrial membrane are cleared by a newly identified quality control pathway involving the conserved eukaryotic protein Msp1 (ATAD1 in humans). Msp1 is a transmembrane AAA-ATPase, but its role in TA protein clearance is not known. Here, using purified components reconstituted into proteoliposomes, we show that Msp1 is both necessary and sufficient to drive the ATP-dependent extraction of TA proteins from the membrane. A crystal structure of the Msp1 cytosolic region modeled into a ring hexamer suggests that active Msp1 contains a conserved membrane-facing surface adjacent to a central pore. Structure-guided mutagenesis of the pore residues shows that they are critical for TA protein extraction in vitro and for functional complementation of an msp1 deletion in yeast. Together, these data provide a molecular framework for Msp1-dependent extraction of mislocalized TA proteins from the outer mitochondrial membrane.

INTRODUCTION

Maintaining the correct intracellular distribution of membrane proteins is essential to the organization of eukaryotic cells. This is accomplished in part through biosynthetic pathways that recognize specific signals in nascent proteins and target them to their correct destination (Chacinska et al., 2009; Heiland and Erdmann, 2005; Inaba and Schnell, 2008; Shao and Hegde, 2011). When these processes fail, quality control pathways help maintain order by identifying damaged or mislocalized membrane proteins and targeting them for degradation (Brodsky and Skach, 2011; Foresti et al., 2014; Hamon et al., 2015; Khmelinskii et al., 2014; Okiyoneda et al., 2010; Tong et al., 2014).

One example of the interplay between biosynthetic and quality control pathways is given by tail-anchored (TA) membrane proteins. TA proteins, which play critical roles in many different cellular processes (Beilharz et al., 2003; Borgese et al., 2007; Wattenberg and Lithgow, 2001), are defined by the presence of a single transmembrane domain (TMD) located near the C terminus (Kutay et al., 1993). Following synthesis, most TA proteins are initially targeted to the endoplasmic reticulum (ER) or the outer mitochondrial membrane (OMM). Targeting to the ER is mediated by the evolutionarily conserved GET pathway (Denic et al., 2013; Hegde and Keenan, 2011; Schuldiner et al., 2008; Stefanovic and Hegde, 2007). Disruption of this pathway results in accumulation of certain ER-destined TA proteins in the OMM (Chen et al., 2014; Jonikas et al., 2009; Okreglak and Walter, 2014; Schuldiner et al., 2008).

Two recent studies have identified the yeast AAA ATPase Msp1 (ATAD1/Thorase in metazoans) as part of a new quality control pathway that eliminates these mislocalized TA proteins from the OMM (Chen et al., 2014; Okreglak and Walter, 2014). Msp1 is a signal-anchored membrane protein comprising an N-terminal TMD that tethers its soluble AAA domain to the cytosolic face of the OMM and peroxisomes (Nakai et al., 1993). In yeast, simultaneous disruption of Msp1 and the GET pathway leads to severe mitochondrial damage, including loss of mitochondrial proteins and DNA, and altered mitochondrial morphology. Similarly, depletion of mammalian ATAD1 compromises mitochondrial function (Chen et al., 2014; Zhang et al., 2011). Nevertheless, how the Msp1 quality control pathway prevents the accumulation of mislocalized TA proteins in the OMM is not known. To address this, we combine biochemical reconstitution with structural analysis to show that a ring hexamer of Msp1 is necessary and sufficient for ATP-dependent extraction of TA proteins from the membrane.

RESULTS

The Minimal Tail-Anchored Protein Extraction Machinery

To investigate whether Msp1 extracts integrated TA proteins from the membrane and to define the minimal number of components required for its activity, we sought to establish an in vitro assay using purified, recombinant proteins (Figure 1A). For this, we devised methods to generate proteoliposomes containing TA proteins and Msp1 in the correct orientation and a soluble chaperone trap to capture dislocated TA proteins for facile isolation.

Full-length recombinant *S. cerevisiae* Msp1 and a model ER TA protein (SumoTMD) (Wang et al., 2010) were co-reconstituted from detergent solution into proteoliposomes with lipid

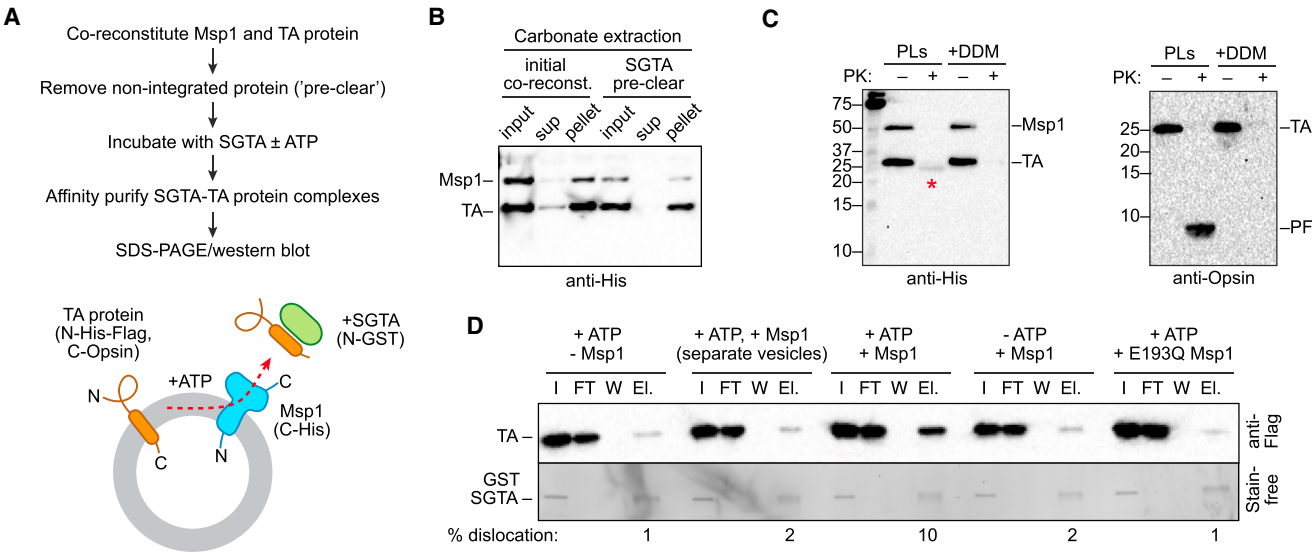

Figure 1. Msp1 Drives ATPase-Dependent TA Protein Dislocation in a Purified System

(A) Assay design. Following co-reconstitution, non-integrated TA proteins are removed by incubation with GST-tagged SGTA and passage over a glutathione-affinity resin. These "pre-cleared" proteoliposomes (PLs) are incubated with ATP and SGTA. SGTA-TA complexes are isolated by glutathione pull-down and analyzed by SDS-PAGE and western blotting. Epitope tags on Msp1 and TA protein are indicated (see also Figure S1).

(B) The presence of non-integrated TA protein before and after pre-clearing was monitored by carbonate extraction, SDS-PAGE, and western blotting. A small amount of non-integrated TA protein is present in the carbonate extraction supernatant immediately following co-reconstitution but not after GST-SGTA pre-clearing.

(C) The orientation of co-reconstituted TA protein and Msp1 in pre-cleared PLs was defined by proteinase K (PK) digestion in the presence or absence of detergent (DDM); products were analyzed by SDS-PAGE and western blotting. In vesicles, the N-terminal 6xHis tag of the TA protein and the C-terminal 6xHis tag of Msp1 are sensitive to digestion, while the C-terminal opsin tag of the TA protein remains protected (PF); this is diagnostic of proper orientation in the proteoliposomes. The red asterisk indicates a minor population of TA protein oriented with its N terminus facing the vesicle lumen.

(D) TA protein dislocation under different conditions. Samples were analyzed by SDS-PAGE and either western blotting (for TA protein) or stain-free gel (for GST-SGTA); the elution and wash fractions correspond to 5× volume equivalents of the input and flow-through fractions. Dislocation efficiencies were estimated using ImageJ. See also Figure S1.

composition mimicking that of the yeast OMM (Kale et al., 2014) (Figure S1). Carbonate extraction of the reconstituted proteoliposomes showed that the majority of TA protein becomes integrated into the bilayer, with only a small amount present in the supernatant (Figure 1B). This putatively non-integrated population of TA protein was removed from the proteoliposomes by binding to GST-tagged SGTA, a TMD-binding chaperone of the eukaryotic cytosol (Wang et al., 2010). Removal of GST-SGTA via a glutathione-affinity resin resulted in "pre-cleared" proteoliposomes in which the TA protein is quantitatively resistant to carbonate extraction (Figure 1B) and thus integrated into the lipid bilayer.

To define the orientation of reconstituted Msp1 and TA protein, we examined the proteinase K (PK) sensitivity of N- and C-terminal epitope tags in pre-cleared proteoliposomes (Figure 1A). Consistent with its in vivo topology, the N-terminal 6xHis tag of the TA protein was sensitive to PK digestion in proteoliposomes, while its C-terminal (lumenal) opsin tag was protected (Figure 1C). Similarly, the C-terminal 6xHis tag of reconstituted Msp1 was sensitive to PK treatment, consistent with exposure of its AAA ATPase domain on the vesicle surface. Thus, both Msp1 and its TA protein client in the pre-cleared proteoliposomes are predominately oriented as they would be in the OMM.

With defined proteoliposomes in hand, we next monitored TA protein extraction under different conditions (Figure 1; Figure S1). In this assay, dislocated TA protein is captured via its exposed TMD by excess GST-SGTA and recovered by glutathione-affinity resin (Figure 1A). Proteoliposomes containing only TA protein and ATP showed background levels of dislocation (~1%–2% of input TA protein), but dislocation was stimulated by ~10-fold (to ~10% of input) in proteoliposomes that also contained Msp1 (Figure 1D). Dislocation was strictly dependent on nucleotide hydrolysis, as no substrate capture was observed in the absence of ATP or when the hydrolysis-deficient Msp1 mutant (E193Q) was used instead of the wild-type protein (Figure 1D). This is consistent with the observation that yeast containing E193Q Msp1 fail to clear mislocalized TA proteins from the OMM (Chen et al., 2014; Okreglak and Walter, 2014).

Dislocation activity increased as a function of time and Msp1 concentration, and no ATP-dependent release of Msp1 from the membrane was observed (Figure S1). Importantly, a mixture of separate Msp1- and TA-only proteoliposomes showed no TA protein dislocation (Figure 1D), illustrating that Msp1 must be in the same membrane as its client. Taken together, these data indicate that Msp1 is the only membrane protein required for ATP-dependent dislocation of a TA protein, thereby defining a minimal reconstituted system for studying this process.

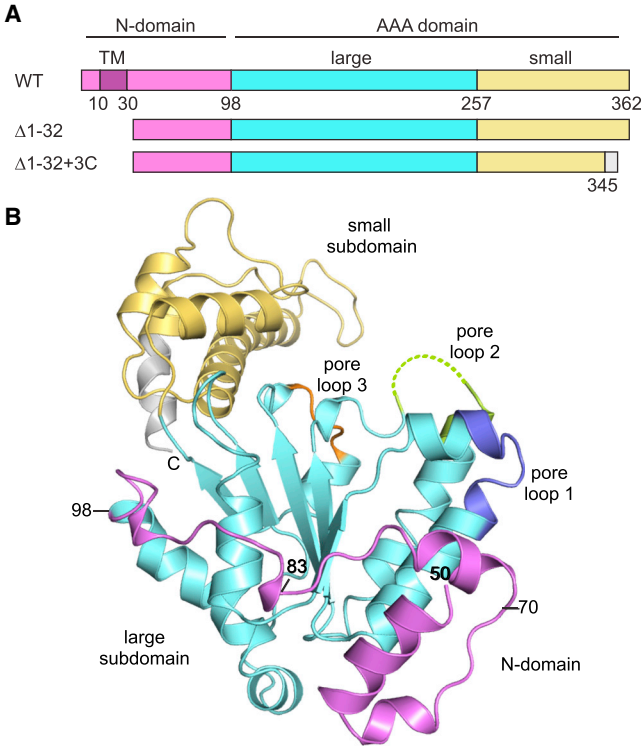

Figure 2. Crystal Structure of Soluble, Nucleotide-free *S. cerevisiae* Msp1

(A) Domain organization of full-length Msp1 (WT), a soluble construct lacking the transmembrane domain (Δ1-32), and the construct used for crystallization (Δ1-32+3C), which contains a 3C protease cleavage site after residue 345; following cleavage, the protein retains an eight-residue scar (gray).

(B) Crystal structure of soluble Msp1 determined in its nucleotide-free, monomeric state. The protein is colored as in (A). The three "pore loops" are highlighted; disordered residues in pore loop 2 are indicated by dotted line. See also Figures S2 and S3 and Table 1.

Table 1. Data Collection and Refinement Statistics

	Selenomet-Msp1 (Δ1-32+3C)
Data Collection	
Space group	*P*3,12
Cell dimensions	
a, *b*, *c* (Å)	56.4, 56.4, 206.7
α, β, γ (°)	90, 90, 120
Wavelength (Å)	0.9792
Resolution (Å)	48.8–2.63 (2.72–2.63)[a]
Redundancy	17.4 (9.4)
Completeness (%)	99 (100)
$I/\sigma I$	9.7 (1.2)
R_{pim} (%)	7.6 (77.1)
$CC_{1/2}$ (%)	99.5 (52.6)
Refinement	
Resolution range (Å)	48.8–2.63
No. Unique Reflections	11,555
R_{work}/R_{free} (%)	23.0/26.0
No. of non-H atoms	
Protein	2,362
Ligands	21
Solvent	11
Average B (Å^2)	
Protein	76.7
Ligands	63.1
Solvent	58.0
RMS Deviations	
Bond lengths (Å)	0.002
Bond angles (°)	0.56
Ramachandran analysis	
Favored (%)	97.0
Allowed (%)	2.7
Outliers (%)	0.0

Data were obtained from a single crystal.

[a]Values in parentheses refer to the high-resolution shell

Crystal Structure of Msp1

To gain insight into Msp1-mediated extraction of TA proteins, we sought to obtain structural information. Initial attempts to crystallize the soluble region of *S. cerevisiae* Msp1 in the presence or absence of nucleotide were unsuccessful. However, a cleaved construct containing a 3C protease site after residue 345 yielded diffraction quality crystals in the nucleotide-free state ("Δ1-32+3C"; Figure 2A). Notably, an otherwise full-length construct of Msp1 containing the same C-terminal truncation retained the ability to complement an msp1 deletion, indicating that the C-terminal region is not strictly required for function in vivo (Figure S2). We solved these crystals at 2.6 Å resolution by single-wavelength anomalous dispersion (Table 1) and found a single copy of Msp1 in the asymmetric unit. Analysis of the crystal packing revealed no hexamer-like interactions.

The structure of the cytosolic Msp1 fragment comprises a helical N-domain and an AAA ATPase domain with characteristic "large" (nucleotide binding) and "small" (helical bundle) subdomains (Figure 2B). Structure-based alignments of the large and small subdomains of Msp1 identified p97/Cdc48, FtsH, and members of the "meiotic" clade of AAA ATPases, including spastin, fidgetin, and Vps4 (Frickey and Lupas, 2004), as the closest structural homologs of Msp1 (Figure S2).

The Msp1 large subdomain contains the canonical Walker A (P loop) and B motifs and is connected to the small subdomain by a short flexible loop (Figure 2B). The small subdomain comprises a four-helix bundle; in some meiotic clade AAA ATPases, functionally important insertions are found between the third and fourth helices of the small subdomain (Peng et al., 2013; Scott et al., 2005). In Msp1, the third helix protrudes from the bundle by virtue of an ~2 turn extension relative to the corresponding helix in closely related homologs (Figure S2); however, the functional significance of this remains unclear, since there is little sequence conservation in this region among Msp1 homologs.

In the nucleotide-free, monomeric Msp1 crystal, the small subdomain is rotated ~180° from its usual position in the ATP-bound state of other AAA ATPases such that the ATP-binding site is not fully formed (Figure S3). The relative orientation of

the large and small subdomains of AAA ATPases typically varies (Stinson et al., 2013), but the "open" conformation observed here is unusual. This may be due to crystal packing forces or truncation of the final 17 C-terminal residues. In certain related AAA ATPases (including spastin and Vps4), these residues pack against the large subdomain; notably, however, truncation of the Msp1 C terminus has no effect on hexamerization or in vivo activity (Figure S2).

A unique structural feature of Msp1 is its N-domain (Figure 2B; Figure S2). The first 16 residues of the crystallized construct, which immediately follow the TMD in the full-length protein, are disordered, likely due to intrinsic flexibility. Residues ~50–80 form a small, three-helix bundle that packs loosely against the large subdomain, and the remainder of the N-domain wraps around the large subdomain in a mostly extended conformation. While the overall sequence conservation of the N-domain is modest, its amphipathic character is conserved and hydrophobic residues throughout the domain help anchor it against the surface of the large subdomain.

Model of the Msp1 Hexameric Ring

Most AAA ATPases function as oligomers. To determine the oligomeric state of the Msp1 cytosolic region, we used size-exclusion chromatography and multi-angle laser light scattering. A soluble Msp1 construct lacking the first 32 residues (Figure S4) exists as a mixture of monomers and dimers in the absence of nucleotide but forms hexamers in the presence of saturating concentrations of the non-hydrolyzable ATP analog, ATPγS (Figure 3A; Figure S4). Likewise, a soluble construct containing the hydrolysis-inactivating mutation E193Q hexamerizes in the presence of ATP (Figure 3A; Figure S4).

We obtained low-resolution structural information on the E193Q hexamer by single-particle cryoelectron microscopy (cryo-EM). In the presence of ATP, Msp1 hexamers are clearly visible (Figure S4); however, because the particles are preferentially oriented, we could not generate high-resolution 3D reconstructions. Nevertheless, 2D class averages generated from nearly 10,000 particles reveal a hexameric ring structure with a diameter of ~13.1 nm and distinctive protrusions emanating from the central ring (Figure 3B).

To generate a pseudo-atomic model of the Msp1 hexamer, we individually superimposed the large and small subdomains of the monomeric crystal structure onto the corresponding subdomains of the D2 ring of hexameric p97 (PDB: 5C18) (Figure S2). The resulting model contains few inter-subunit steric clashes, and these would presumably be relieved by subtle conformational changes accompanying ATP binding and hexamer formation. Within the hexameric assembly, the large and small subdomains are arranged in approximately the same plane, while the N-domain lies below this plane, along what is likely the membrane proximal surface of Msp1 (Figure 3C). Consistent with the 2D class averages, the elongated small subdomain protrudes outward from the center of the ring, giving the overall assembly a longest dimension of ~13.4 nm. The Msp1 hexamer model has a well-formed ATP-binding site with the characteristic "second region of homology" (SRH) of "meiotic clade" AAA ATPases (Frickey and Lupas, 2004) close to the nucleotide-binding pocket of the adjacent subunit.

To further validate the model, we sought to disrupt the predicted hexamer interface by site-directed mutagenesis. We identified a hydrophobic interface between the large subdomain of one subunit and the small subdomain of an adjacent subunit (Figure 3D) and introduced a double leucine-to-aspartate mutation at positions 122 and 123. Using a soluble, ATPase-deficient construct containing the double mutation, we observed reduced hexamer formation in the presence of ATP (Figure 3E). Likewise, a full-length Msp1 construct containing the double mutation was unable to complement an *msp1* deletion in vivo (Figure 3F) and failed to extract TA substrate in vitro (Figure 3G). Taken together, these data validate the structural model and indicate that Msp1 functions as a ring hexamer.

To locate functionally important surfaces, we mapped electrostatic potential and sequence conservation from 94 fungal Msp1 homologs to the surface of the hexamer model. The positive charge character of the "bottom" surface of the hexamer (including the N-domain) is compatible with the negatively charged surface of the OMM, supporting assignment of this face as the membrane proximal surface of the Msp1 hexamer (Figure S4). Most of the hexamer periphery, including the N-domain and small subdomain, shows limited sequence conservation (Figure 3C). In contrast, the "top" and bottom surfaces, particularly toward the center of the ring, are highly conserved, suggesting a role in the capture and extraction of TA substrates.

Functional Role of the Central Pore

Many AAA ATPases translocate polypeptide substrates through their central pore, a process that involves a highly conserved aromatic-hydrophobic-glycine pore loop motif (Martin et al., 2008). In Msp1, the central pore is lined with conserved residues from three loops (Figure 4A). Loop 1 contains the canonical "WYG" sequence and is well defined in the crystal structure of the Msp1 monomer (Figure 4B). In the hexamer, loop 1 lies on the membrane proximal side, adjacent to the N-domain at the pore entrance. Loop 2, comprising mostly polar and charged side chains, lies at the center of the pore. Although residues 200–205 are disordered in the crystal structure, loop 2 residues contribute to the main constriction point of the pore, separating the membrane-proximal and cytosolic-facing vestibules. Loop 3, enriched in negatively charged sidechains, lies on the cytosolic-facing side of the ring.

To explore the role of the Msp1 pore loops, we generated two double mutants—W166A/Y167A in loop 1 and H206A/E207A in loop 2—and tested their activity. In each case, the double mutants failed to complement an *msp1* deletion in yeast, although the loop 1 mutant was more severe than the loop 2 mutant (Figure 4C). Likewise, both mutants failed to extract TA protein in vitro (Figure 4D). This loss of activity is not due to impaired hexamer formation, as soluble, ATPase-deficient constructs containing the double pore loop mutations formed hexamers in the presence of ATP (Figure S4F). Taken together, these data point to an essential functional role for the central pore, most likely involving TA substrate translocation during extraction from the membrane.

Functional Role of the N-domain

The Msp1 N-domain comprises a lumenal sequence of ~10 residues, an ~20 residue TMD, and a cytosolic ~68 residue linker that tethers the AAA domain to the OMM (Figures 2A and 5A).

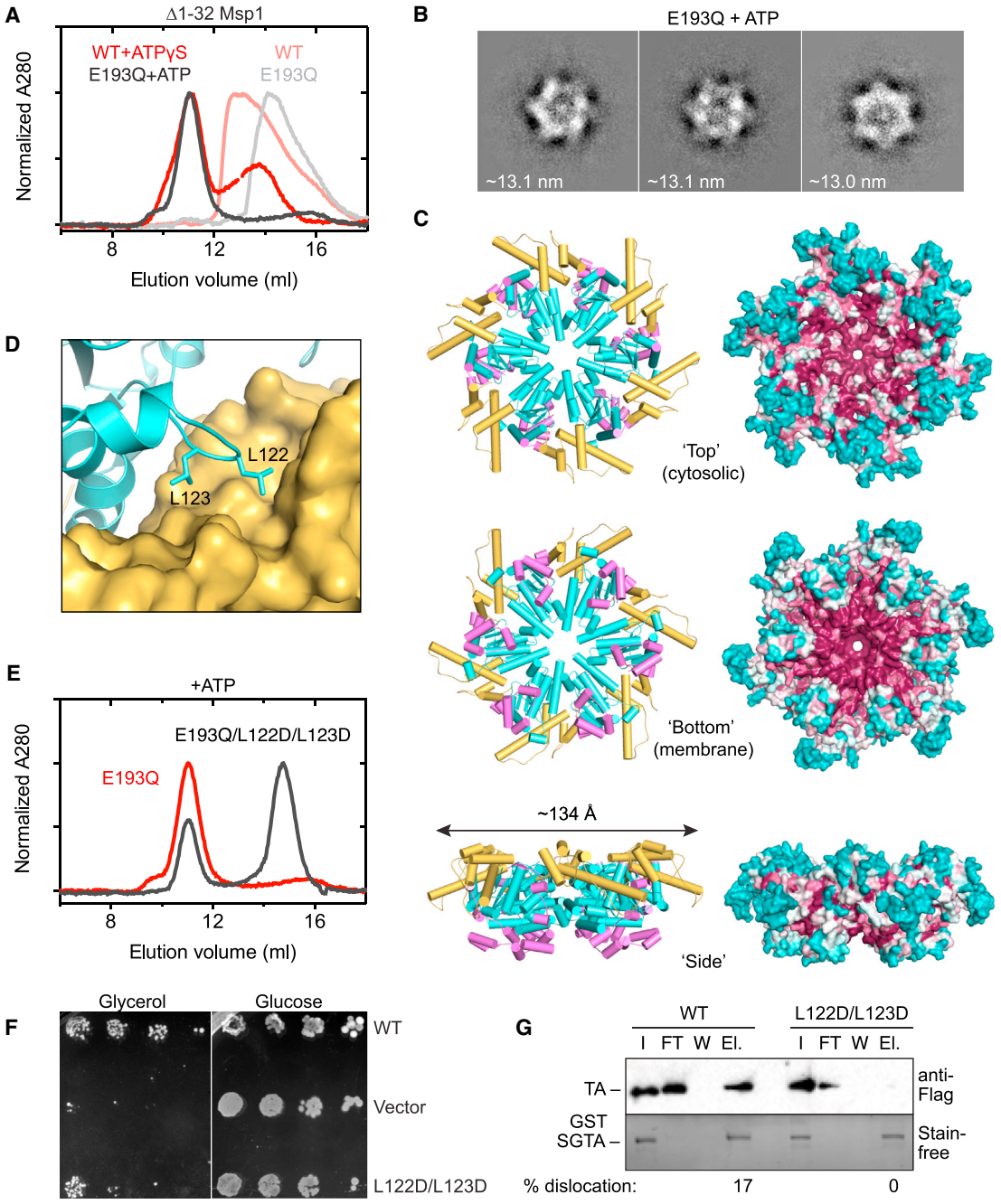

Figure 3. Msp1 Functions as a Ring Hexamer

(A) Size-exclusion chromatography (SEC) of wild-type (WT) Δ1-32 Msp1 and its ATPase-deficient mutant (E193Q) demonstrates ATPγS- and ATP-dependent hexamer formation (see also Figure S4).

(B) Cryo-EM 2D class averages of 1 mg/mL Δ1-32 Msp1E193Q incubated with Mg^{2+}ATP reveal a hexameric structure with distinct protrusions emanating from the central ring.

(C) A hexameric model generated by separately superimposing the large and small subdomains of Msp1 with the corresponding subdomains in the D2 ring of hexameric, ATP-bound human p97 (PDB: 5C18) (see also Figures S2–S4); colored as in Figure 2. At right, the sequence conservation of 94 fungal Msp1 proteins is mapped to the molecular surface of the Msp1 hexamer model from most (magenta) to least (cyan) conserved. Note that the sequence conservation is strongest on the "bottom" (membrane proximal) face of the hexamer and in the central pore.

(D) Closeup of a portion of the predicted hexamer interface between hydrophobic residues in the large subdomain of one subunit (cyan) and the small subdomain of a second subunit (yellow).

(E) SEC analysis shows that a double mutation within this interface (L122D/L123D) disrupts hexamerization of the soluble E193Q construct.

(F and G) The corresponding mutations in full-length, wild-type Msp1 also disrupt function in vivo (F) and in vitro (G). See also Figure S4.

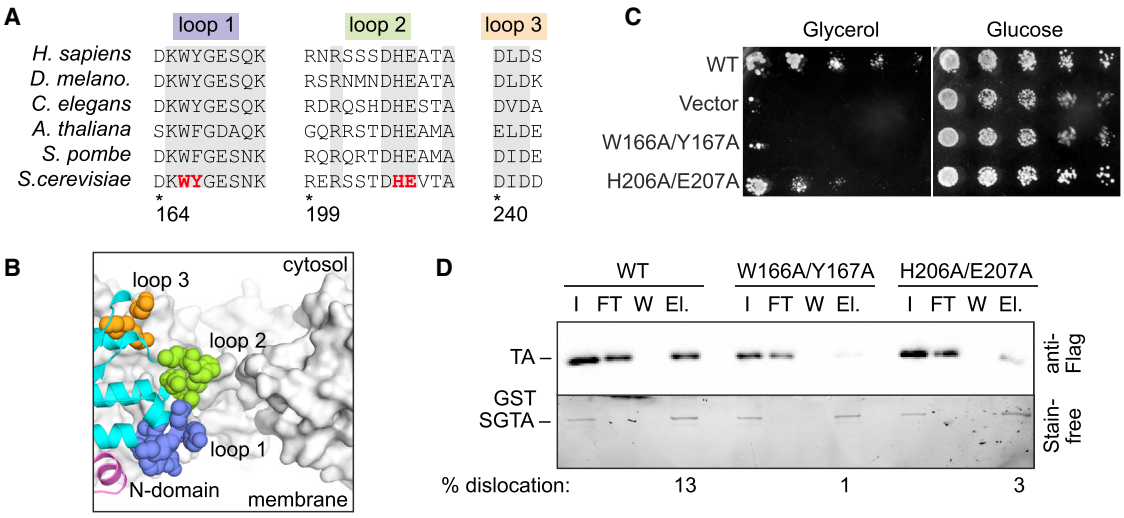

Figure 4. Central Pore Loop Mutations Disrupt TA Protein Dislocation

(A) Alignment of pore loop sequences in homologs from yeast Msp1 to human ATAD1. The most conserved residues are highlighted in gray; residues mutated for functional analysis in yeast Msp1 are in red.

(B) Cutaway of the central pore in the hexamer model. Three subunits are shown, two in surface representation (gray) and the third in cartoon with pore loop residues shown as spheres. Note the constriction in center of the pore by residues in pore loop 2 (some of which are disordered in the crystal and thus not shown); this constriction separates the membrane proximal and cytosolic faces of Msp1.

(C and D) Mutation of conserved residues in pore loops 1 and 2 disrupts activity of full-length Msp1 in vivo (C) and in vitro (D) but does not disrupt ATP-dependent hexamer formation by the soluble domain. See also Figure S4.

Residues within these regions are not strongly conserved in Msp1, but the linker region has been implicated in substrate binding in related AAA ATPases (Monroe and Hill, 2016; Wohlever et al., 2014). Given this and its location at the entrance to the central pore, we sought to clarify the role of the Msp1 linker. We constructed a series of deletion mutants (Figure 5A) and found that the linker region is largely dispensable for function in vivo; indeed, removing the entire linker (Δ32-98) resulted in only a slight defect in vivo (Figure 5B) and in vitro (Figure 5C). Thus, consistent with its lack of sequence conservation, the N-domain linker region of Msp1 is not strictly required for function.

Next, we investigated the role of the N-domain TMD by generating chimeric constructs in which the Msp1 TMD and lumenal region were swapped with the corresponding regions from yeast Tom70 or human stannin, unrelated single-pass membrane proteins of the OMM with the same topology as Msp1. The Tom70 chimera localized to the OMM (Figure S5) and complemented the *msp1* deletion in vivo (Figure 5D). In contrast, the stannin chimera failed to target properly to the OMM (Figure S5) and thus failed to complement in vivo (Figure 5D). However, using the in vitro extraction assay, where localization is artificially imposed, we found that both chimeras were functional for extraction (Figure 5E). Thus, while TA protein extraction does not appear to depend on the precise sequence of the Msp1 TMD, the TMD is required for proper targeting and anchoring of Msp1 to the OMM.

DISCUSSION

Here we provide direct evidence that Msp1 extracts TA proteins from the membrane. Using reconstituted proteoliposomes containing only recombinant Msp1 and an integrated model ER TA protein, we show that TA proteins are completely extracted from the bilayer in an ATPase-dependent process (Figure 1). This extraction activity is fully encoded in Msp1 and does not require additional factors or post-translational modification, including ubiquitination or proteolysis.

Our functional and structural data provide insight into the mechanism of extraction. First, Msp1 appears to function as ATP-dependent ring hexamer. Thus, mutations that disrupt the Msp1 hexamer in vitro also disrupt its ability to extract TA proteins from the membrane (Figure 3). Whether Msp1 forms a constitutive hexamer in vivo or assembles in a regulated process is not clear. An intriguing possibility is that the unusual open conformation observed in the monomeric, nucleotide-free crystal structure of Msp1 (Figure 2; Figure S3) represents an inactive ground-state conformation, allowing for regulated activation of Msp1 through conformational switching.

Second, the central pore appears to play a critical role in TA protein binding and/or translocation during extraction. Thus, mutations within the conserved pore loops, which do not impair hexamer formation (Figure S4F), disrupt the ability of Msp1 to extract TA proteins from the bilayer (Figure 4). Third, despite its location near the entrance to the central pore, the N-domain linker region is largely dispensable for function (Figure 4). Finally, the N-terminal TMD is minimally required for localization and anchoring of Msp1 to the OMM. The observation that membrane protein extraction can occur in the presence of a heterologous TMD sequence (Figure 5) is similar to that reported for the bacterial AAA+ protease FtsH (Akiyama and Ito, 2000). Notably, while dispensable for proteolysis of soluble clients, the TMDs of FtsH and the mitochondrial protease m-AAA (Korbel et al.,

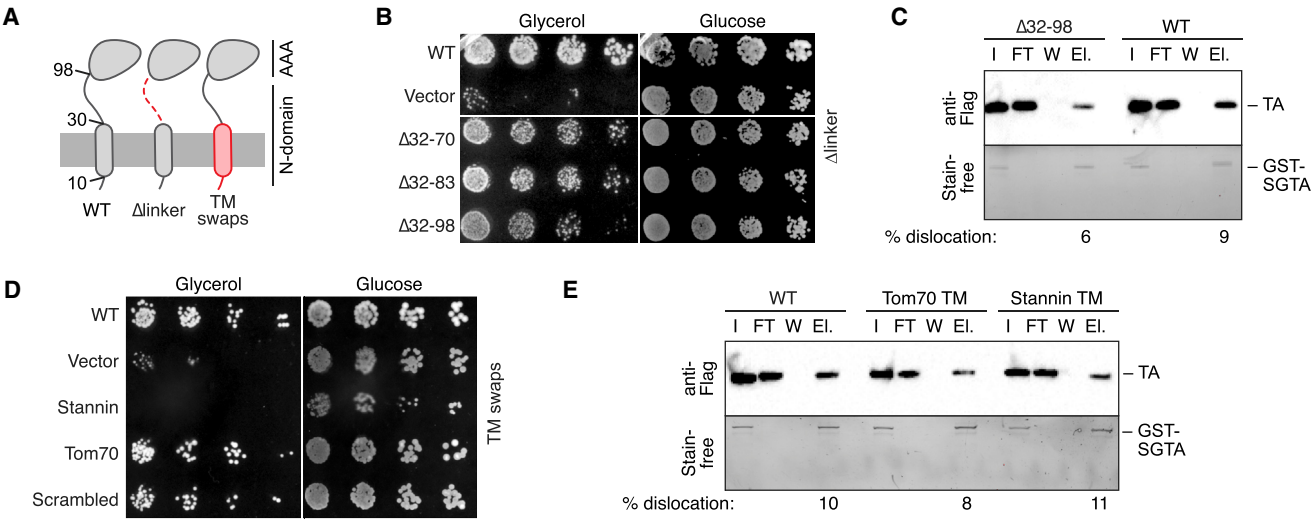

Figure 5. Role of the N-domain Linker and TM Regions

(A) Schematic of the N-domain constructs used for functional analysis.

(B and C) Progressive deletion of the N-domain linker ("Δlinker") connecting the Msp1 AAA domain to its TM has little effect on in vivo (B) or in vitro (C) activity; a slight reduction in activity is observed for the longest deletion (Δ32-98). Note that all samples were grown on the same plate.

(D) Chimeric constructs ("TM swaps"), in which the Msp1 TM sequence is scrambled or swapped with the TM from yeast Tom70 or human Stannin, show differing effects on activity in vivo; whereas the scrambled and Tom70 TM chimeras are functional, the Stannin chimera mislocalizes (Figure S5) and thus fails to complement.

(E) In vitro, however, the Tom70 and Stannin chimeras are both functional for extraction. See also Figure S5.

2004) are required for extraction of their integral membrane protein clients. An intriguing possibility is that the TMDs of these membrane-anchored dislocases form channel-like structures or perturb the bilayer around a client to facilitate extraction from the bilayer.

How Msp1 selects TA membrane protein clients for extraction remains unclear. This is a challenging task because sequence differences between the TMDs of mislocalized and endogenous TA proteins are likely to be subtle, and genuine clients are likely to be rare relative to the number of endogenous TA proteins. Although heterologous sequences can functionally substitute for the Msp1 TMD, the TMD may play an active role in substrate selection by sensing hydrophobic mismatch or surfaces that become exposed in the absence of appropriate binding partners. While our data show that Msp1 functions autonomously to extract TA proteins in vitro, additional factors may play a role in substrate selection in vivo. Systematic analyses are needed to define how the cell ensures that only genuine substrates are extracted; these studies will be facilitated by our in vitro assay.

The immediate fate of TA proteins following extraction also remains unclear. During ER-associated degradation (ERAD), the cytosolic chaperone Bag6 (BCL2-associated athanogene 6) is recruited to the ER to capture aggregation-prone clients extracted by the Cdc48/p97 AAA+ ATPase (Claessen and Ploegh, 2011; Kawahara et al., 2013; Lee and Ye, 2013; Wang et al., 2011). Intriguingly, the cytosolic-facing surface of the Msp1 hexamer is conserved, suggesting a potential binding site for a cytosolic chaperone to rapidly engage TA protein clients during extraction from the membrane.

In addition to extracting mislocalized TA proteins from the OMM, the Msp1/ATAD1 AAA ATPases may perform additional functions in the cell. This is suggested by the broad subcellular distribution of Msp1/ATAD1, including the OMM, peroxisomes, plasma membrane, and the cytosol. By analogy with the membrane-anchored AAA+ proteases FtsH, i-AAA, and m-AAA, whose clients include peripheral and integral membrane protein (Graef et al., 2007; Ito and Akiyama, 2005; Korbel et al., 2004), Msp1/ADAD1 AAA ATPases likely act on different classes of substrates. Consistent with this, putative non-TA protein clients have been identified for yeast Msp1 (Chen et al., 2014), while mammalian ATAD1 has been proposed to mediate internalization of AMPA receptor complexes by dissociating a peripherally associated cytosolic factor from the receptor (Zhang et al., 2011). Future studies are needed to define how Msp1/ATAD1 family members function in different cellular contexts.

STAR★METHODS

Detailed methods are provided in the online version of this paper and include the following:

- KEY RESOURCES TABLE
- CONTACT FOR REAGENT AND RESOURCE SHARING
- EXPERIMENTAL MODEL AND SUBJECT DETAILS
  - NovaBlue Cells
  - BL21-DE3 pRIL Cells
  - W303-1a Yeast
- METHOD DETAILS
  - Production of Soluble Protein Constructs
  - Crystallization and Data Collection
  - Structure Determination, Refinement, and Analysis
  - Electron Microscopy and Image Analysis

SUPPLEMENTAL INFORMATION

Supplemental Information includes five figures and can be found with this article online at http://dx.doi.org/10.1016/j.molcel.2017.06.019.

AUTHOR CONTRIBUTIONS

M.L.W and R.J.K. conceived of the project and designed experiments. M.L.W. performed all experiments with help from other authors. A.M. assisted with crystallization and data collection, SEC experiments, and cryo-EM sample preparation. P.T.M. performed cryo-EM data collection and analysis. R.J.K. assisted with X-ray structure determination. K.J.D. assisted with the yeast complementation assays and microscopy. M.L.W. and R.J.K. wrote the paper with input from all authors.

ACKNOWLEDGMENTS

We thank J. Grubb, J. Austin, III, P. Rodriguez, R. Hegde, and B. Glick for technical assistance; members of the Bezanilla, Perozo, and Keenan labs for instrumentation and discussions; and V. Denic for the SumoTMD construct. We acknowledge support from the NE-CAT (24-IDE) beamline staff; NE-CAT is supported by NIH grant P41 GM103403 and NIH-ORIP HEI grant (S10 RR029205). APS is a U.S. Department of Energy (DOE) Office of Science User Facility operated for the DOE Office of Science by Argonne National Laboratory under Contract No. DE-AC02-06CH11357. We acknowledge support from J. Remis and the Structural Biology Facility at Northwestern University, the Robert H. Lurie Comprehensive Cancer Center of Northwestern University, and NCI CCSG P30 CA060553. We thank the Chicago Biomedical Consortium and the Searle Funds at The Chicago Community Trust and the support of the University of Chicago Research Computing Center. This work was also supported by NIH grant 2R01GM086487-05 to R.J.K.; M.L.W. was supported by NIH training grants 2T32HL7381-36A1 and 5T32CA9594-25 and an NIH postdoctoral fellowship, 1F32GM119194-01. P.T.M. and K.J.D. were supported by NIH training grant T32 GM007183.

Received: January 13, 2017
Revised: May 9, 2017
Accepted: June 16, 2017
Published: July 13, 2017

REFERENCES

Adams, P.D., Afonine, P.V., Bunkóczi, G., Chen, V.B., Davis, I.W., Echols, N., Headd, J.J., Hung, L.W., Kapral, G.J., Grosse-Kunstleve, R.W., et al. (2010). PHENIX: a comprehensive Python-based system for macromolecular structure solution. Acta Crystallogr. D Biol. Crystallogr. *66*, 213–221.

Akiyama, Y., and Ito, K. (2000). Roles of multimerization and membrane association in the proteolytic functions of FtsH (HflB). EMBO J. *19*, 3888–3895.

Beilharz, T., Egan, B., Silver, P.A., Hofmann, K., and Lithgow, T. (2003). Bipartite signals mediate subcellular targeting of tail-anchored membrane proteins in Saccharomyces cerevisiae. J. Biol. Chem. *278*, 8219–8223.

Bell, J.M., Chen, M., Baldwin, P.R., and Ludtke, S.J. (2016). High resolution single particle refinement in EMAN2.1. Methods *100*, 25–34.

Borgese, N., Brambillasca, S., and Colombo, S. (2007). How tails guide tail-anchored proteins to their destinations. Curr. Opin. Cell Biol. *19*, 368–375.

Brodsky, J.L., and Skach, W.R. (2011). Protein folding and quality control in the endoplasmic reticulum: Recent lessons from yeast and mammalian cell systems. Curr. Opin. Cell Biol. *23*, 464–475.

Chacinska, A., Koehler, C.M., Milenkovic, D., Lithgow, T., and Pfanner, N. (2009). Importing mitochondrial proteins: machineries and mechanisms. Cell *138*, 628–644.

Chen, Y.C., Umanah, G.K., Dephoure, N., Andrabi, S.A., Gygi, S.P., Dawson, T.M., Dawson, V.L., and Rutter, J. (2014). Msp1/ATAD1 maintains mitochondrial function by facilitating the degradation of mislocalized tail-anchored proteins. EMBO J. *33*, 1548–1564.

Claessen, J.H., and Ploegh, H.L. (2011). BAT3 guides misfolded glycoproteins out of the endoplasmic reticulum. PLoS ONE *6*, e28542.

Denic, V., Dötsch, V., and Sinning, I. (2013). Endoplasmic reticulum targeting and insertion of tail-anchored membrane proteins by the GET pathway. Cold Spring Harb. Perspect. Biol. *5*, a013334.

Emsley, P., Lohkamp, B., Scott, W.G., and Cowtan, K. (2010). Features and development of Coot. Acta Crystallogr. D Biol. Crystallogr. *66*, 486–501.

Evans, P. (2006). Scaling and assessment of data quality. Acta Crystallogr. D Biol. Crystallogr. *62*, 72–82.

Fitzgerald, I., and Glick, B.S. (2014). Secretion of a foreign protein from budding yeasts is enhanced by cotranslational translocation and by suppression of vacuolar targeting. Microb. Cell Fact. *13*, 125.

Foresti, O., Rodriguez-Vaello, V., Funaya, C., and Carvalho, P. (2014). Quality control of inner nuclear membrane proteins by the Asi complex. Science *346*, 751–755.

Frickey, T., and Lupas, A.N. (2004). Phylogenetic analysis of AAA proteins. J. Struct. Biol. *146*, 2–10.

Gietz, R.D., and Woods, R.A. (2002). Transformation of yeast by lithium acetate/single-stranded carrier DNA/polyethylene glycol method. Methods Enzymol. *350*, 87–96.

Glaser, F., Pupko, T., Paz, I., Bell, R.E., Bechor-Shental, D., Martz, E., and Ben-Tal, N. (2003). ConSurf: identification of functional regions in proteins by surface-mapping of phylogenetic information. Bioinformatics *19*, 163–164.

Goldstein, A.L., and McCusker, J.H. (1999). Three new dominant drug resistance cassettes for gene disruption in Saccharomyces cerevisiae. Yeast *15*, 1541–1553.

Graef, M., Seewald, G., and Langer, T. (2007). Substrate recognition by AAA+ ATPases: distinct substrate binding modes in ATP-dependent protease Yme1 of the mitochondrial intermembrane space. Mol. Cell. Biol. *27*, 2476–2485.

Hamon, M.P., Bulteau, A.L., and Friguet, B. (2015). Mitochondrial proteases and protein quality control in ageing and longevity. Ageing Res. Rev. *23* (Pt A), 56–66.

Hegde, R.S., and Keenan, R.J. (2011). Tail-anchored membrane protein insertion into the endoplasmic reticulum. Nat. Rev. Mol. Cell Biol. *12*, 787–798.

Heiland, I., and Erdmann, R. (2005). Biogenesis of peroxisomes. Topogenesis of the peroxisomal membrane and matrix proteins. FEBS J. *272*, 2362–2372.

Inaba, T., and Schnell, D.J. (2008). Protein trafficking to plastids: one theme, many variations. Biochem. J. *413*, 15–28.

Ito, K., and Akiyama, Y. (2005). Cellular functions, mechanism of action, and regulation of FtsH protease. Annu. Rev. Microbiol. *59*, 211–231.

Jonikas, M.C., Collins, S.R., Denic, V., Oh, E., Quan, E.M., Schmid, V., Weibezahn, J., Schwappach, B., Walter, P., Weissman, J.S., and Schuldiner, M. (2009). Comprehensive characterization of genes required for protein folding in the endoplasmic reticulum. Science *323*, 1693–1697.

Kale, J., Chi, X., Leber, B., and Andrews, D. (2014). Examining the molecular mechanism of bcl-2 family proteins at membranes by fluorescence spectroscopy. Methods Enzymol. *544*, 1–23.

Kawahara, H., Minami, R., and Yokota, N. (2013). BAG6/BAT3: emerging roles in quality control for nascent polypeptides. J. Biochem. *153*, 147–160.

Khmelinskii, A., Blaszczak, E., Pantazopoulou, M., Fischer, B., Omnus, D.J., Le Dez, G., Brossard, A., Gunnarsson, A., Barry, J.D., Meurer, M., et al. (2014). Protein quality control at the inner nuclear membrane. Nature *516*, 410–413.

Korbel, D., Wurth, S., Käser, M., and Langer, T. (2004). Membrane protein turnover by the m-AAA protease in mitochondria depends on the transmembrane domains of its subunits. EMBO Rep. *5*, 698–703.

Kutay, U., Hartmann, E., and Rapoport, T.A. (1993). A class of membrane proteins with a C-terminal anchor. Trends Cell Biol. *3*, 72–75.

Lee, J.G., and Ye, Y. (2013). Bag6/Bat3/Scythe: a novel chaperone activity with diverse regulatory functions in protein biogenesis and degradation. BioEssays *35*, 377–385.

Martin, A., Baker, T.A., and Sauer, R.T. (2008). Pore loops of the AAA+ ClpX machine grip substrates to drive translocation and unfolding. Nat. Struct. Mol. Biol. *15*, 1147–1151.

Mateja, A., Paduch, M., Chang, H.Y., Szydlowska, A., Kossiakoff, A.A., Hegde, R.S., and Keenan, R.J. (2015). Protein targeting. Structure of the Get3 targeting factor in complex with its membrane protein cargo. Science *347*, 1152–1155.

Monroe, N., and Hill, C.P. (2016). Meiotic clade AAA ATPases: protein polymer disassembly machines. J. Mol. Biol. *428* (9 Pt B), 1897–1911.

Nakai, M., Endo, T., Hase, T., and Matsubara, H. (1993). Intramitochondrial protein sorting. Isolation and characterization of the yeast MSP1 gene which belongs to a novel family of putative ATPases. J. Biol. Chem. *268*, 24262–24269.

Okiyoneda, T., Barrière, H., Bagdány, M., Rabeh, W.M., Du, K., Höhfeld, J., Young, J.C., and Lukacs, G.L. (2010). Peripheral protein quality control removes unfolded CFTR from the plasma membrane. Science *329*, 805–810.

Okreglak, V., and Walter, P. (2014). The conserved AAA-ATPase Msp1 confers organelle specificity to tail-anchored proteins. Proc. Natl. Acad. Sci. USA *111*, 8019–8024.

Papanikou, E., Day, K.J., Austin, J., and Glick, B.S. (2015). COPI selectively drives maturation of the early Golgi. eLife *4*, 4.

Peng, W., Lin, Z., Li, W., Lu, J., Shen, Y., and Wang, C. (2013). Structural insights into the unusually strong ATPase activity of the AAA domain of the Caenorhabditis elegans fidgetin-like 1 (FIGL-1) protein. J. Biol. Chem. *288*, 29305–29312.

Schneider, C.A., Rasband, W.S., and Eliceiri, K.W. (2012). NIH Image to ImageJ: 25 years of image analysis. Nat. Methods *9*, 671–675.

Schuldiner, M., Metz, J., Schmid, V., Denic, V., Rakwalska, M., Schmitt, H.D., Schwappach, B., and Weissman, J.S. (2008). The GET complex mediates insertion of tail-anchored proteins into the ER membrane. Cell *134*, 634–645.

Scott, A., Chung, H.Y., Gonciarz-Swiatek, M., Hill, G.C., Whitby, F.G., Gaspar, J., Holton, J.M., Viswanathan, R., Ghaffarian, S., Hill, C.P., and Sundquist, W.I. (2005). Structural and mechanistic studies of VPS4 proteins. EMBO J. *24*, 3658–3669.

Shao, S., and Hegde, R.S. (2011). Membrane protein insertion at the endoplasmic reticulum. Annu. Rev. Cell Dev. Biol. *27*, 25–56.

Sievers, F., Wilm, A., Dineen, D., Gibson, T.J., Karplus, K., Li, W., Lopez, R., McWilliam, H., Remmert, M., Söding, J., et al. (2011). Fast, scalable generation of high-quality protein multiple sequence alignments using Clustal Omega. Mol. Syst. Biol. *7*, 539.

Stefanovic, S., and Hegde, R.S. (2007). Identification of a targeting factor for posttranslational membrane protein insertion into the ER. Cell *128*, 1147–1159.

Stinson, B.M., Nager, A.R., Glynn, S.E., Schmitz, K.R., Baker, T.A., and Sauer, R.T. (2013). Nucleotide binding and conformational switching in the hexameric ring of a AAA+ machine. Cell *153*, 628–639.

Tong, Z., Kim, M.S., Pandey, A., and Espenshade, P.J. (2014). Identification of candidate substrates for the Golgi Tul1 E3 ligase using quantitative diGly proteomics in yeast. Mol. Cell. Proteomics *13*, 2871–2882.

Van Duyne, G.D., Standaert, R.F., Karplus, P.A., Schreiber, S.L., and Clardy, J. (1993). Atomic structures of the human immunophilin FKBP-12 complexes with FK506 and rapamycin. J. Mol. Biol. *229*, 105–124.

Wach, A., Brachat, A., Pöhlmann, R., and Philippsen, P. (1994). New heterologous modules for classical or PCR-based gene disruptions in Saccharomyces cerevisiae. Yeast *10*, 1793–1808.

Wang, F., Brown, E.C., Mak, G., Zhuang, J., and Denic, V. (2010). A chaperone cascade sorts proteins for posttranslational membrane insertion into the endoplasmic reticulum. Mol. Cell *40*, 159–171.

Wang, Q., Liu, Y., Soetandyo, N., Baek, K., Hegde, R., and Ye, Y. (2011). A ubiquitin ligase-associated chaperone holdase maintains polypeptides in soluble states for proteasome degradation. Mol. Cell *42*, 758–770.

Wattenberg, B., and Lithgow, T. (2001). Targeting of C-terminal (tail)-anchored proteins: understanding how cytoplasmic activities are anchored to intracellular membranes. Traffic *2*, 66–71.

Winter, G. (2010). Xia2: an expert system for macromolecular crystallography data reduction. J. Appl. Cryst. *43*, 186–190.

Wohlever, M.L., Baker, T.A., and Sauer, R.T. (2014). Roles of the N domain of the AAA+ Lon protease in substrate recognition, allosteric regulation and chaperone activity. Mol. Microbiol. *91*, 66–78.

Zhang, J., Wang, Y., Chi, Z., Keuss, M.J., Pai, Y.M., Kang, H.C., Shin, J.H., Bugayenko, A., Wang, H., Xiong, Y., et al. (2011). The AAA+ ATPase Thorase regulates AMPA receptor-dependent synaptic plasticity and behavior. Cell *145*, 284–299.

Zhang, Z.R., Bonifacino, J.S., and Hegde, R.S. (2013). Deubiquitinases sharpen substrate discrimination during membrane protein degradation from the ER. Cell *154*, 609–622.

STAR★METHODS

KEY RESOURCES TABLE

REAGENT or RESOURCE	SOURCE	IDENTIFIER
Antibodies		
Rabbit polyclonal anti-Flag (1:12,000 dilution)	Sigma-Aldrich	Cat. #F7425; RRID: AB_439687
Bovine polyclonal HRP anti-Rabbit (1:10,000 dilution)	Santa Cruz	Cat. #sc-2370; RRID: AB_634837
Mouse monoclonal HRP anti-Penta-His (1:1,500 dilution)	QIAGEN	Cat. #34460; RRID: AB_2619735
Mouse monoclonal anti-Opsin (1:4,000 dilution)	Abcam	Cat. #ab98887; RRID: AB_10696805
Rabbit polyclonal anti-Mouse (1:5,000 dilution)	Abcam	Cat. #ab6728; RRID: AB_955440
Bacterial and Virus Strains		
E. coli NovaBlue competent cells	Novagen	Cat. #70181
E. coli BL21 (DE3) pRIL competent cells	Agilent	Cat. #230245
Chemicals, Peptides, and Recombinant Proteins		
Criterion Gels, TGX Stain Free, 4%–20% 26 wells	Bio-Rad	Cat. #5678095
Immobilon-P Transfer Membrane (PVDF)	Millipore	Cat. #IPVH00010
Pierce ECL Western Blotting Substrate	Thermo Scientific	Cat. #32106
SuperSignal West Femto Maximum Senstivity Substrate	Thermo Scientific	Cat. #34095
n-dodecyl-β-D-maltoside	bioWORLD	Cat. #40430017
Deoxy Big Chaps	Anatrace	Cat. #B310
Chicken egg phosphatidyl choline	Avanti	Cat. #840051C
Chicken egg phosphatidyl ethanolamine	Avanti	Cat. #840021C
Bovine liver phosphatidyl inositol	Avanti	Cat. #840042C
Synthetic DOPS	Avanti	Cat. #840035C
Synthetic TOCL	Avanti	Cat. #710335C
Glutathione Agarose Spin Columns	Thermo Scientific	Cat. #PI16103
Seleno-DL-methionine	Sigma-Aldrich	Cat. #S3875
50% PEG 3350	Hampton	Cat. #HR2-527
8 M Sodium Thiocyanate	Hampton	Cat. #HR2-245
C-Flat holey carbon grids (CF-1.2/1.3-2C)	EMS	Cat. #CF213-25
Adenosine-5 ft.-O-(3-Thiotriphosphate), tetralithium salt	EMD Millipore	Cat. #119120
Adenosine 5' Triphosphate disodium salt	Acros Organics	Cat. #102800100
MitoTracker Red CMXRos	Thermo Scientific	Cat. #M7512
Biobeads	Bio-Rad	Cat. #152-3920
Deposited Data		
Atomic coordinates and structure factors	This study	PDB: 5W0T
Raw data (gels, blots, plates, microscopy)	This study	http://dx.doi.org/10.17632/5xyf82bz5z.1
Experimental Models: Organisms/Strains		
S. cerevisiae: W303-1, get3::NAT, msp1::KanMX,	This study	N/A
Recombinant DNA		
His_6-TEV-Δ1-32 Msp1 (pET28a)	This study	N/A
Δ1-32+3C Msp1-His_6 (pET21b)	This study	N/A
Msp1-His_6 (pET21b)	This study	N/A
Msp1 ± 1 kb (YCplac33)	This study	N/A
Msp1-GFP ± 1 kb (YCplac33)	This study	N/A
His_6-$Flag_3$-Sumo-Sec22 TMD-Opsin (pET28a)	Wang et al., 2010	N/A
GST-SGTA (pGEX6p1)	Mateja et al., 2015	N/A

(*Continued on next page*)

Continued

REAGENT or RESOURCE	SOURCE	IDENTIFIER
Software and Algorithms		
Xia2 DIALS	Evans, 2006 Winter, 2010	http://dials.diamond.ac.uk
PHENIX	Adams et al., 2010	http://www.phenix-online.org/
COOT	Emsley et al., 2010	https://www2.mrc-lmb.cam.ac.uk/personal/pemsley/coot/
Clustal Omega	Sievers et al., 2011	http://www.ebi.ac.uk/
Consurf	Glaser et al., 2003	http://consurf.tau.ac.il
Pymol	N/A	http://www.pymol.org
ImageJ	Schneider et al., 2012	https://imagej.nih.gov/ij/
Eman 2.1	Bell et al., 2016	http://blake.bcm.edu/emanwiki/EMAN2
Expasy	N/A	www.expasy.org

CONTACT FOR REAGENT AND RESOURCE SHARING

Further information and requests for resources and reagents should be directed to and will be fulfilled by the Lead Contact, Robert Keenan (bkeenan@uchicago.edu).

EXPERIMENTAL MODEL AND SUBJECT DETAILS

NovaBlue Cells

For cloning, *E. coli* NovaBlue competent cells were transformed according to the manual provided by the manufacturer and grown on LB agar plates at 37°C overnight.

BL21-DE3 pRIL Cells

For protein expression, *E. coli* BL21(DE3) containing a pRIL plasmid and a protein expression vector were grown in terrific broth at 37°C until an OD_{600} of 0.6-1.0. Cultures were induced with isopropyl-1-thio-β-D-galactopyranoside (IPTG) at a final concentration of 1 mM and grown at room temperature for an additional 3-4 hr.

Selenomethionine (Se-Met) labeled protein was expressed in M9 minimal media with 0.4% glucose, 2 mM $MgSO_4$, and 0.1 mM $CaCl_2$. Culture was grown at 37°C until an OD_{600} of 0.6, at which point isoleucine, leucine, lysine, phenylalanine, threonine, and valine were added to a final concentration of 100 mg/L to inhibit methionine biosynthesis (Van Duyne et al., 1993). Culture was incubated at 37°C for an additional 15 min, before adding IPTG and Se-Met to a final concentration of 1 mM and 60 mg/L respectively. The culture was grown at room temperature for an additional 3.5 hr.

W303-1a Yeast

S. cerevisiae W303-1a (*MATa*, *his3*, *leu2*, *met15*, *trp1*, *ura3*), with Msp1 and Get3 disrupted by the KanMX4 or natMX4 cassettes respectively, was used in this study. Standard PCR-based homologous recombination was used to generate all mutant strains (Wach et al., 1994). Briefly, drug selection cassette (KanMX4 or NatMX4) flanked with 40-45 bp fragments binding to *msp1* gene or upstream and downstream of *get3* was PCR amplified and transformed into the wild-type W303-1a (Gietz and Woods, 2002; Goldstein and McCusker, 1999). Gene deletions were confirmed by PCR. After generating the double knockout in haploids, cells were mated with W303-1α to form a diploid strain and transformed with the appropriate vector. Haploid strains containing the double knockout and plasmid were generated by sporulation and tetrad analysis. Media used in this study was SD-Ura, which contained 0.5% ammonium sulfate, 0.079% CSM minus Ura, 0.17% yeast nitrogen base, and 2% of either glucose or glycerol). Yeast strains were grown at 30°C.

METHOD DETAILS

Production of Soluble Protein Constructs

Msp1

The gene encoding the soluble region of *S. cerevisiae* Msp1 (Δ1-32) was PCR amplified from genomic DNA and subcloned into a pET28a derivative (Novagen) encoding an N-terminal 6xHis tag followed by a TEV or 3C protease cleavage site. All insertions and deletions were performed by standard PCR techniques. Site-specific mutagenesis was carried out by QuickChange PCR. All constructs were verified by DNA sequencing.

Plasmids encoding the soluble region of *S. cerevisiae* Msp1 (Δ1-32) or its mutants were transformed into *E. coli* BL21(DE3) containing a pRIL plasmid and expressed in terrific broth at 37°C until an OD_{600} of 0.6-1.0, cultures were induced with 1 mM IPTG and grown at room temperature for an additional 3-4 hr. Cells were harvested by centrifugation, and resuspended in Msp1 Lysis Buffer (20 mM Tris pH 7.5, 100 mM NaCl, 20 mM Imidazole, 0.01 mM EDTA, 1 mM DTT) supplemented with 0.05 mg/mL lysozyme (Sigma), 1 mM phenylmethanesulfonyl fluoride (PMSF) and 500 U of benzonase (Sigma), and lysed by sonication. The supernatant was isolated by centrifugation for 40 min at 4°C at 18,500 x g and purified by Ni-NTA affinity chromatography (Novagen) on a gravity column. Ni-NTA resin was washed with 10 column volumes (CV) of Msp1 Lysis Buffer and then 10 CV of Wash Buffer (Msp1 Lysis buffer with 30 mM Imidazole) before elution with Lysis Buffer supplemented with 250 mM imidazole.

The protein was further purified by size exclusion chromatography (SEC) (Superdex 200 Increase 10/300 GL, GE Healthcare) in 20 mM Tris pH 7.5, 100 mM NaCl, 0.1 mM TCEP. Peak fractions were pooled, concentrated to 5-15 mg/ml in a 30 kDa MWCO Amicon Ultra centrifugal filter (Millipore) and aliquots were flash-frozen in liquid nitrogen and stored at –80°C. Protein concentrations were determined by A_{280} using a calculated extinction coefficient (Expasy) for monomeric samples or a Bradford assay (samples containing nucleotide). The soluble E193Q construct was purified similarly, but with an additional overnight dialysis step (against 20 mM Tris pH 7.5, 200 mM NaCl, 0.1 mM EDTA, 1 mM DTT) to remove any bound nucleotide before SEC.

The crystallization construct (Δ1-32+3C) was generated by subcloning the soluble region of *S. cerevisiae* Msp1 (Δ1-32) into a pET21b derivative containing a C-terminal 6xHis tag, and then inserting a 3C protease site after residue 345. This construct was expressed and purified as described above with the following changes. After Ni-NTA purification, 3C protease was added at a 1:100 molar ratio to Msp1 and dialyzed for 16 hr at 4°C against 20 mM Tris pH 7.5, 150 mM NaCl, 5 mM βME. Uncleaved protein and 3C protease were then removed by subtractive Ni-NTA chromatography. Cleaved protein was further purified by SEC on an S200 Increase column equilibrated in Buffer B (20 mM HEPES pH 7.5, 100 mM NaCl, 1 mM DTT). Selenomethionine (Se-Met) labeled protein was purified similarly, except for an additional 16 hr dialysis step against Buffer B after SEC.

GST-SGTA

GST-tagged SGTA was expressed and purified as described previously (Mateja et al., 2015; Wang et al., 2010). Briefly, cells were harvested by centrifugation, and resuspended in SGTA Lysis Buffer (50 mM HEPES pH 7.5, 150 mM NaCl, 0.01 mM EDTA, 1 mM DTT, 10% glycerol) supplemented with 0.05 mg/mL lysozyme (Sigma), 1 mM PMSF and 500 U of benzonase (Sigma), and lysed by sonication. The supernatant was isolated by centrifugation for 40 min at 4°C at 18,500 x g and purified by Glutathione affinity chromatography (Gold Bio) on a gravity column. Resin was washed with 20 column volumes (CV) of SGTA Lysis Buffer and then eluted with 3 CV of SGTA Lysis Buffer supplemented with 10 mM reduced glutathione. The protein was further purified by size exclusion chromatography (SEC) (Superdex 200 Increase 10/300 GL, GE Healthcare) in 20 mM Tris pH 7.5, 100 mM NaCl, 0.1 mM TCEP. Peak fractions were pooled, concentrated to 10 mg/ml in a 50 kDa MWCO Amicon Ultra centrifugal filter (Milipore) and aliquots were flash-frozen in liquid nitrogen and stored at –80°C. Protein concentrations were determined by A_{280} using a calculated extinction coefficient (Expasy).

Crystallization and Data Collection

Native and selenomethioine-containing Msp1 crystals were grown at room temperature by hanging drop vapor diffusion. A protein solution containing ~9 mg/mL protein was mixed in a 1:1 (2:1 for Se-Met) ratio with a reservoir solution containing 16% PEG 3350 and 0.6 M Sodium Thiocyanate. Crystals were cryoprotected in 16% PEG 3350, 0.6 M Sodium Thiocyanate, 20% ethylene glycol, and flash frozen in liquid nitrogen.

Native and selenium SAD data were collected at 100K at APS beamline 24-IDC (λ = 0. 97918 Å) on a Pilatus 6M pixel-array detector. Data were processed using the *xia2* DIALS pipeline (Evans, 2006; Winter, 2010); data collection and processing statistics are listed in Table 1.

Structure Determination, Refinement, and Analysis

The 2.6 Å structure of the Msp1 soluble region (Δ1-32+3C) was determined by SAD using PHENIX (Adams et al., 2010); after phasing and density modification the resulting electron density maps were of good quality, allowing 242 residues to be placed automatically using Autobuild. The initial model was improved by manual building and refinement with COOT (Emsley et al., 2010) and PHENIX. The final model contains one Msp1 and 11 water molecules; no electron density was observed for residues 33-49 and 200-205. Refinement and validation statistics are listed in Table 1.

Sequence conservation was analyzed from an alignment of 94 fungal Msp1 homologs identified by a BLASTp search (NCBI) using *S. cerevisiae* Msp1 as the search sequence. After aligning in Clustal Omega (Sievers et al., 2011) (http://www.ebi.ac.uk/), sequence conservation was mapped to the surface of Msp1 using the ConSurf server (Glaser et al., 2003) (http://consurf.tau.ac.il). Structure figures were generated with PyMOL (http://www.pymol.org).

Electron Microscopy and Image Analysis

For cryo-EM, 2 μl of soluble (Δ1-32) *S. cerevisiae* Msp1 E193Q at 1 mg/ml was incubated for 30 s on glow discharged C-Flat holey carbon grids (CF-1.2/1.3-2C, EMS), blotted for 10 s at 100% humidity and plunge frozen in liquid ethane using an FEI Vitrobot. Cryo-EM samples were imaged using a JEOL 3200FS operating at 300 KeV, equipped with a K2 direct electron detector camera (Gatan). Images were collected manually at a nominal magnification of 30,000x with a pixel size of 1.19Å and defocus range of

2-4 μm. Total exposure time was 4 s with an accumulated dose of 48 $e^-/Å^2$. Particle selection, CTF correction, 2D class averaging, and measurements were performed in EMAN 2.1 (Bell et al., 2016) on the University of Chicago Midway computing cluster. Cryo-EM 2D class averages were calculated from 9,897 particles picked from 77 micrographs. Diameter measurements were made automatically with ImageJ (Schneider et al., 2012) after highlighting by applying a grayscale threshold to the class averages.

Size Analysis by Size-Exclusion Chromatography and Multi-angle Laser Light Scattering

Analytical SEC was carried out on a Superdex 200 Increase 10/300 GL column (GE Healthcare) with 500 μL of 2 mg/mL protein supplemented with 2 mM of the appropriate nucleotide and 2 mM $MgCl_2$, as needed. Unless indicated otherwise, the column was equilibrated in 20 mM Tris pH 7.5, 100 mM NaCl, 0.1 mM TCEP; nucleotide and $MgCl_2$ were not present in the SEC running buffer.

For size analysis by SEC-MALS, 100 μL of 10 mg/mL protein sample were injected onto a Superdex 200 10/300 GL column (GE Healthcare) equilibrated in 20 mM Tris pH 7.5, 100 mM NaCl, 0.1 mM TCEP. The purification system was coupled to an online, static, light scattering detector (Dawn HELEOS II, Wyatt Technology), a refractive-index detector (Optilab rEX, Wyatt Technology), and an ultraviolet-light detector (UPC-900, GE Healthcare). Absolute weight-averaged molar masses were calculated using the ASTRA software (Wyatt Technology).

Yeast Studies

Complementation Assay

For complementation assays in *S. cerevisiae*, full-length Msp1 with the flanking upstream and downstream 1000 bp was amplified from genomic DNA and subcloned into a YCplac33 vector. For cellular localization studies, msGFP (Fitzgerald and Glick, 2014) was cloned onto the C terminus of Msp1 in a YCplac33 vector modified to include AsiSI and NotI restriction sites in frame with the C terminus of Msp1.

Complementation was performed essentially as described (Chen et al., 2014). Briefly, haploid W303-1 cells containing the appropriate plasmid were grown overnight in SD-Ura with 2% glucose. Cultures were diluted to the same OD_{600}, serially diluted 3x or 4x in SD-Ura with 2% glucose, stamped onto SD-Ura plates containing either 2% glucose or 2% glycerol, and grown at 30°C. To control for variability in the assay, a positive control (wild-type) and negative control (empty vector) were included on every plate. Images are representative of $N > 2$ trials.

Localization Studies

Localization studies were performed with GFP-tagged Msp1 on a YCplac33 plasmid in diploid W303-1 *S. cerevisiae*, which were haploid for *chromosomal msp1* and *get3*. Yeast cultures were grown in SD-Ura medium overnight and then 1 mL of culture was mixed with 10 μL of 10 μM MitoTracker Red CMXRos (Thermo Scientific). Culture was incubated at 30°C for 15 min, pelleted, washed in SD-Ura, and then resuspended in SD-Ura. Static images were captured with living cells that were compressed beneath a coverslip without fixation and then immediately viewed. To capture static images by widefield microscopy, we used an Axioplan2 epifluorescence microscope (Zeiss) equipped with a 1.4-NA 100x Plan Apo objective and a digital camera (Hamamatsu) (Papanikou et al., 2015). ImageJ (Schneider et al., 2012) was used to colorize, adjust brightness, and merge the images.

Production of Membrane Proteins

SumoTMD

The vector for bacterial expression of SumoTMD (Sec22 TMD fused to Sumo) was a gift from Vlad Denic, and was expressed and purified as previously described (Mateja et al., 2015; Wang et al., 2010). Briefly, after transforming the SumoTMD plasmid into *E. coli* BL21(DE3)/pRIL, the cells were grown in terrific broth at 37°C until an OD_{600} of 0.6-0.8, and then induced with 0.4 mM IPTG and grown at 37°C for an additional 3-4 hr. Cells were harvested by centrifugation, and resuspended in SumoTMD Lysis Buffer (50 mM Tris pH 7.5, 300 mM NaCl, 10 mM $MgCl_2$, 10 mM Imidazole, 10% glycerol) supplemented with 0.05 mg/mL lysozyme (Sigma), 1 mM PMSF and 500 U of benzonase (Sigma), and lysed by sonication. Membrane proteins were solubilized by addition of n-dodecyl-β-D-maltoside (DDM) to a final concentration of 1% and rocked at 4°C for 30'. Lysate was cleared by centrifugation for at 4°C for 1 hr at 35,000 x g and purified by Ni-NTA affinity chromatography.

Ni-NTA resin was washed with 10 column volumes (CV) of SumoTMD Wash Buffer 1 (50 mM Tris pH 7.5, 500 mM NaCl, 10 mM $MgCl_2$, 10 mM imidazole, 5 mM β-mercaptoethanol (BME), 10% glycerol, 0.1% DDM). Resin was then washed with 10 CV of SumoTMD Wash Buffer 2 (same as Wash Buffer 1 except with 300 mM NaCl and 25 mM imidazole) and 10 CV of SumoTMD Wash Buffer 3 (same as Wash Buffer 1 with 150 mM NaCl and 50 mM imidazole) and then eluted with 3 CV of SumoTMD Elution Buffer (same as Wash Buffer 3 except with 250 mM imidazole).

The protein was further purified by size exclusion chromatography (SEC) (Superdex 200 Increase 10/300 GL, GE Healthcare) in 50 mM Tris pH 7.5, 150 mM NaCl, 10 mM $MgCl_2$, 5 mM BME, 10% glycerol, 0.1% DDM. Peak fractions were pooled, aliquots were flash-frozen in liquid nitrogen and stored at –80°C. Protein concentrations were determined by A_{280} using a calculated extinction coefficient (Expasy).

Msp1

Full-length *S. cerevisiae* Msp1 was PCR amplified from genomic DNA, subcloned into a pET21b derivative with a C-terminal 6xHis tag and expressed as described above for the soluble constructs. Cells were lysed by passing three times through a high-pressure

microfluidizer and the insoluble fraction was harvested by centrifugation for 1 hr at 4°C at 140,000 x g. After resolubilizing for 16 hr in Msp1 Lysis Buffer containing 1% DDM (Bioworld), the detergent-soluble supernatant was isolated by centrifugation for 45 min at 140,000 x g and purified by Ni-NTA affinity chromatrography and SEC as described above for the soluble constructs, except that all buffers contained 0.05% DDM. Peak fractions were concentrated in 100 kDa MWCO Amicon Ultra centrifugal filter (Millipore). Protein concentrations were determined by A_{280} using a calculated extinction coefficient (Expasy) and aliquots were flash frozen in liquid nitrogen.

Reconstitution of Msp1 Activity in Proteoliposomes

Liposome Preparation

Liposomes mimicking the lipid composition of the yeast outer mitochondrial membrane were prepared as described (Kale et al., 2014). Briefly, a 25 mg lipid film was prepared by mixing chloroform stocks of chicken egg phosphatidyl choline (Avanti 840051C), chicken egg phosphatidyl ethanolamine (Avanti 840021C), bovine liver phosphatidyl inositol (Avanti 840042C), synthetic DOPS (Avanti 840035C), and synthetic TOCL (Avanti 710335C) at a 48:28:10:10:4 molar ratio with 1 mg of DTT. Chloroform was evaporated under a gentle steam of nitrogen and then left on a vacuum (< 1 mTorr) overnight. Lipid film was resuspended in Liposome Buffer (50 mM HEPES KOH pH 7.5, 15% glycerol, 1 mM DTT) to a final concentration of 20 mg/mL and then subjected to five freeze-thaw cycles with liquid nitrogen. Liposomes were extruded 15 times through a 200 nm filter at 60°C, distributed into single use aliquots, and flash frozen in liquid nitrogen.

Proteoliposome Preparation

Proteoliposomes were prepared by mixing 800 nM Msp1, 670 nM TA protein (SumoTMD), and 2 mg/mL liposomes in Reconstitution Buffer (50 mM HEPES KOH pH 7.5, 200 mM potassium acetate, 7 mM magnesium acetate, 2 mM DTT, 10% sucrose, 0.01% sodium azide, and 0.1% deoxy big chaps) (Zhang et al., 2013). Detergent was removed by adding 25 mg of biobeads and rotating the samples for 16 hr at 4°C. After removing biobeads, unincorporated TA protein was pre-cleared by incubating the reconstituted material with excess (5 μM) GST-SGTA and passing over a glutathione spin column (Pierce #16103); the flow through was collected and used immediately for dislocation assays. Reconstitution efficiency of Msp1 and TA protein was monitored by SDS-PAGE and anti-His western blot, and found to vary by ~3-fold and ~2-fold for Msp1 and TA protein, respectively (Figure S1A).

Dislocation Assay

Dislocation assays contained 60 μL of pre-cleared proteoliposomes, 5 μM GST-SGTA, and 2 mM ATP and the final volume was adjusted to 200 μL with Extraction Buffer (50 mM HEPES KOH pH 7.5, 200 mM potassium acetate, 7 mM magnesium acetate, 2 mM DTT). Samples were incubated at 30°C for 35 min and then loaded onto a glutathioine spin column. Columns were washed 4x with Extraction Buffer and eluted with the same buffer supplemented with 20 mM glutathione pH 8.5. Samples were loaded onto stain free gels, imaged, and then transferred to a PVDF membrane and blotted as indicated in the Key Resources Table. Load volumes were normalized by the amount of reconstituted Msp1 (Figure S1A). To account for variability in reconstitution efficiency and western blotting, a new reconstitution and dislocation assay with wild-type Msp1 was done in parallel with each mutant Msp1. Figures are representative of N > 3 separate reconstitutions. Dislocation efficiencies were estimated using ImageJ (Schneider et al., 2012).

For the dislocation time course (Figure S1C), start times for the assay were staggered such that all assays ended at 30 min. Samples were kept on ice until ATP was added to initiate the assay, at which point samples were incubated at 30°C.

Carbonate Extraction Assay

For carbonate extraction, Msp1 and TA protein were co-reconstituted into liposomes as described above. After removing biobeads, samples were treated as described Figure 1, diluted 2x with 100 mM sodium carbonate pH 11.5 and incubated on ice for 15 min. The membrane-associated fraction was pelleted by spinning for 45 min at 100,000 rpm in a TLA 120.1 rotor. The pellet was resuspended in an equal volume of 1% SDS.

Protease Protection Assay

Protease protection assay was carried out in a 10 μL total volume with 8 μL of pre-cleared proteoliposomes, 1 μL of 5 mg/mL proteinase K and 0.05% DDM (where indicated). Samples were incubated on ice for 1 hr and then 0.5 μL of freshly prepared 500 mM PMSF was added. The 10 μL reaction was then reverse quenched into 90 μL of boiling 1% SDS and incubated at 95°C for 10 min.

QUANTIFICATION AND STATISTICAL ANALYSIS

Western blot band intensities were estimated using ImageJ (Schneider et al., 2012). Reconstitution efficiency of Msp1 and TA protein was monitored by SDS-PAGE and anti-His western blot and found to vary by ~3-fold and ~2-fold respectively (Figure S1A). To account for variability in reconstitution efficiency and western blotting, a new reconstitution and dislocation assay with wild-type Msp1 was done in parallel with each Msp1 mutant. Figures are representative of N > 3 separate reconstitutions. Dislocation efficiency was quantified by comparing the amount TA protein in the "elution" lane with the amount of substrate in the "input" lane. Note that the "input" lane is diluted 5x relative to the "elution" lane.

To control for variability in the yeast complementation assay, a positive control (wild-type) and a negative control (empty vector) were included on every plate. Images for yeast complementation assays are representative of N > 2 trials.

DATA AND SOFTWARE AVAILABILITY

The unprocessed image files used to prepare the figures in this manuscript are deposited in Mendeley Data and are available at http://dx.doi.org/10.17632/5xyf82bz5z.1. The atomic coordinates and structure factors for the soluble *S. cerevisiae* Msp1 monomer are deposited in the PDB: 5W0T.

Molecular Cell, Volume *67*

Supplemental Information

Msp1 Is a Membrane Protein Dislocase for Tail-Anchored Proteins

Matthew L. Wohlever, Agnieszka Mateja, Philip T. McGilvray, Kasey J. Day, and Robert J. Keenan

SUPPLEMENTAL INFORMATION

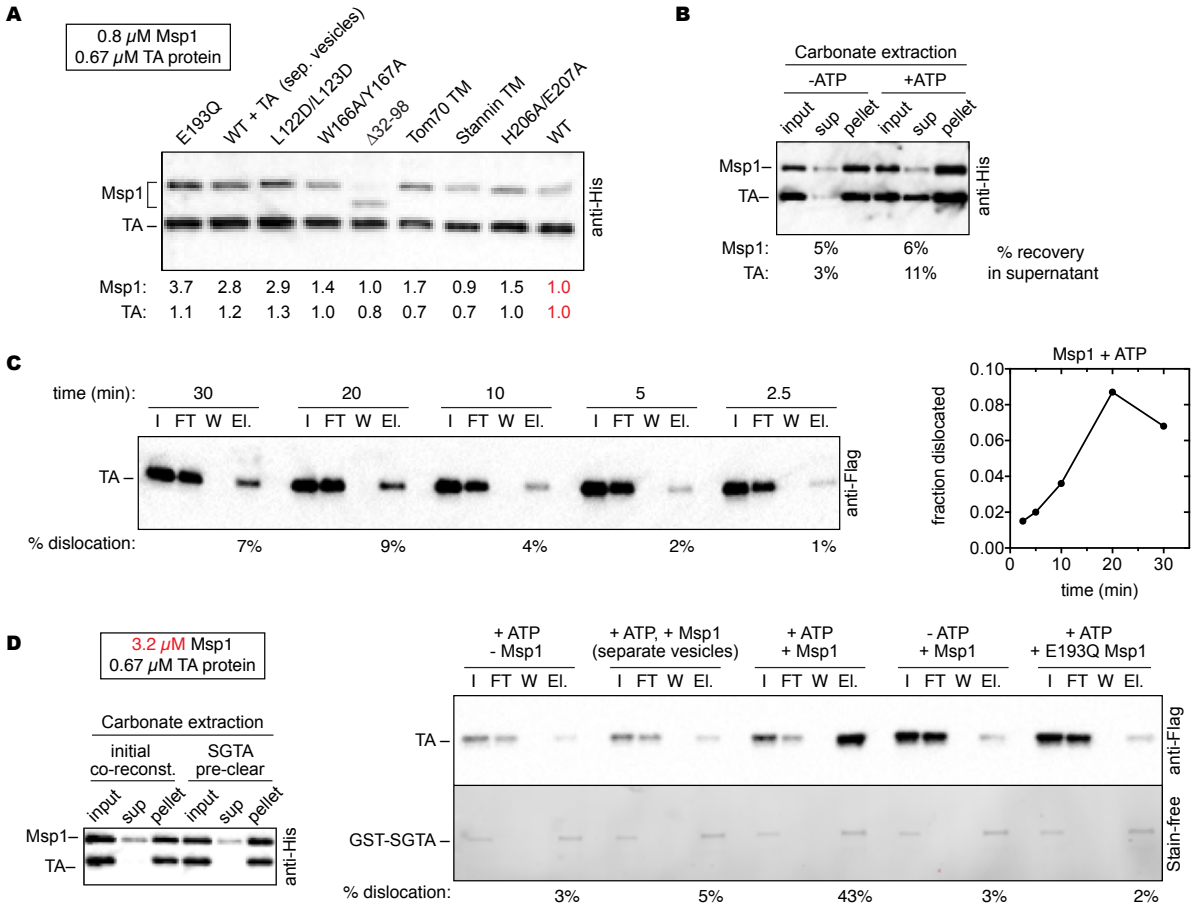

Figure S1, related to Figure 1. Additional characterization of the dislocation assay. (A) Following co-reconstitution with 0.67 μM TA protein and 0.8 μM of the indicated Msp1 construct, proteoliposomes were pre-cleared (see Figure 1B) and the relative amount of integrated Msp1 and SumoTMD was quantified by SDS-PAGE and anti-His western blotting. Band intensities were estimated using ImageJ. Relative levels vary by less than four- and two-fold for Msp1 and TA protein, respectively. (B) Anti-His western blot of a dislocation assay monitored by carbonate extraction instead of GST-SGTA pull-down. Here, a small amount of unincorporated Msp1 is observed in the carbonate supernatant (corresponding to residual Msp1 that sometimes remains after pre-clearing); importantly, it does not accumulate in an ATP-dependent manner. In contrast, TA protein does accumulate in the carbonate supernatant in an ATP-dependent manner. Thus, the proteoliposomes remain intact throughout the ATP-dependent dislocation reaction, and Msp1 itself is not dislocated from the proteoliposomes. (C) Time course of protein dislocation by wild-type Msp1, monitored by anti-Flag western blot. (D) A protein dislocation assay using proteoliposomes reconstituted with four-fold higher concentrations of Msp1 (3.2 μM instead of 0.8 μM). Under these conditions, very little non-integrated TA protein is detected in the carbonate extractable supernatant (left panel). In the presence of ATP, more than 40% of the TA protein is dislocated; this increased efficiency presumably reflects the larger number of proteoliposomes containing Msp1 hexamers.

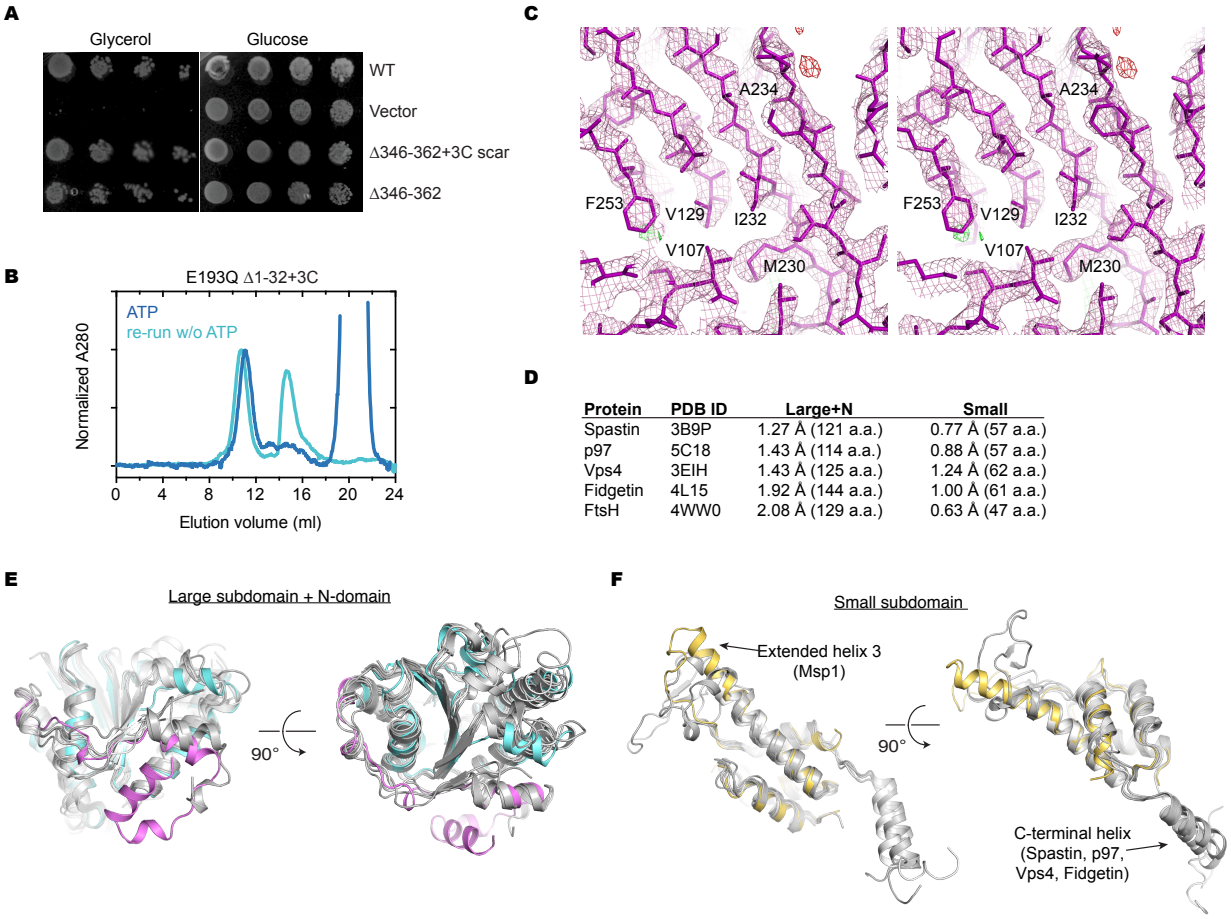

Figure S2, related to Figure 2. Characterization of the crystallization construct (Δ1-32+3C) and structural comparison. (A) Full-length Msp1 constructs truncated at position 345 and either containing (Δ346-362 + 3C scar) or lacking (Δ346-362) the 8-residue 3C protease cleavage site scar complement an Msp1 knockout in yeast. (B) Gel filtration analysis of an ATPase-deficient form of the crystallization construct following cleavage with 3C protease. This construct forms ATP-dependent hexamers (dark blue trace). Re-running the main peak in buffer lacking ATP demonstrates the reversibility of hexamer formation (light blue trace). (C) Cross-eyed stereo view of σA-weighted 2*F*o-*F*c (pink) and *F*o-*F*c (green, red) electron density maps, calculated at 2.6 Å and contoured at 1.5 and 3.5 sigma, respectively. A portion of the final refined model, including part of the central beta sheet in the Msp1 large subdomain, is superimposed (magenta sticks). (D) RMSD (on Cα) for five of the closest structural homologs of *S. cerevisiae* Msp1. The number of residues included in the alignment is given in parentheses. (E) Structural overlap of the Msp1 large subdomain (cyan) and N-domain (magenta), with the homologs in (D). (F) As in (E), but with the Msp1 small subdomain (yellow). The extended helix 3 of Msp1 is highlighted here; in some meiotic-clade AAA ATPases, this region contains functionally important insertions. The C-terminal helix of other meiotic-clade members is also highlighted; this region is not present in the Msp1 soluble construct crystallized in this work.

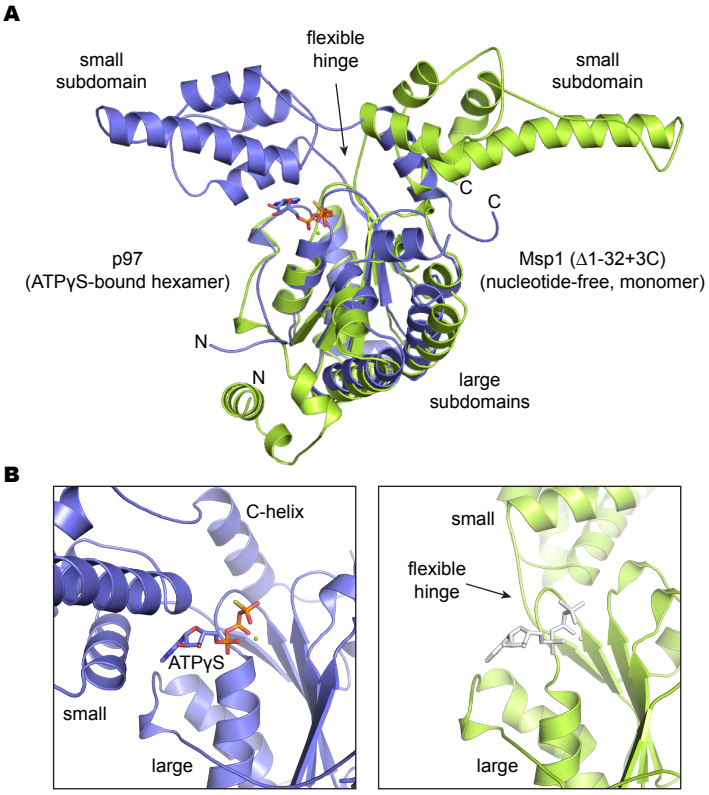

Figure S3, related to Figure 2. Conformation of the Msp1 small subdomain observed in the nucleotide-free, monomeric crystal. (A) Structural overlap highlights the unusual ~180° rotation of the Msp1 (green) small subdomain observed in the monomeric, nucleotide-free crystal relative to its position in hexameric, ATPγS-bound p97 (blue). (B) In the crystallized conformation, the nucleotide binding site of Msp1 is only partially formed. Closeup of the composite ATP binding sites of p97 (left panel), which was crystallized as an ATPγS-bound hexamer, and Msp1 (right panel) which was crystallized as a nucleotide-free monomer; for reference, an ATPγS molecule was modeled into the monomeric Msp1 active site (grey). Whether the open conformation represent a physiologically relevant on-pathway conformation that could be exploited to regulate Msp1 activity, or simply reflects the interdomain flexibility seen in many AAA+ ATPases (here captured in an unusual conformation by crystal packing forces), remains to be clarified.

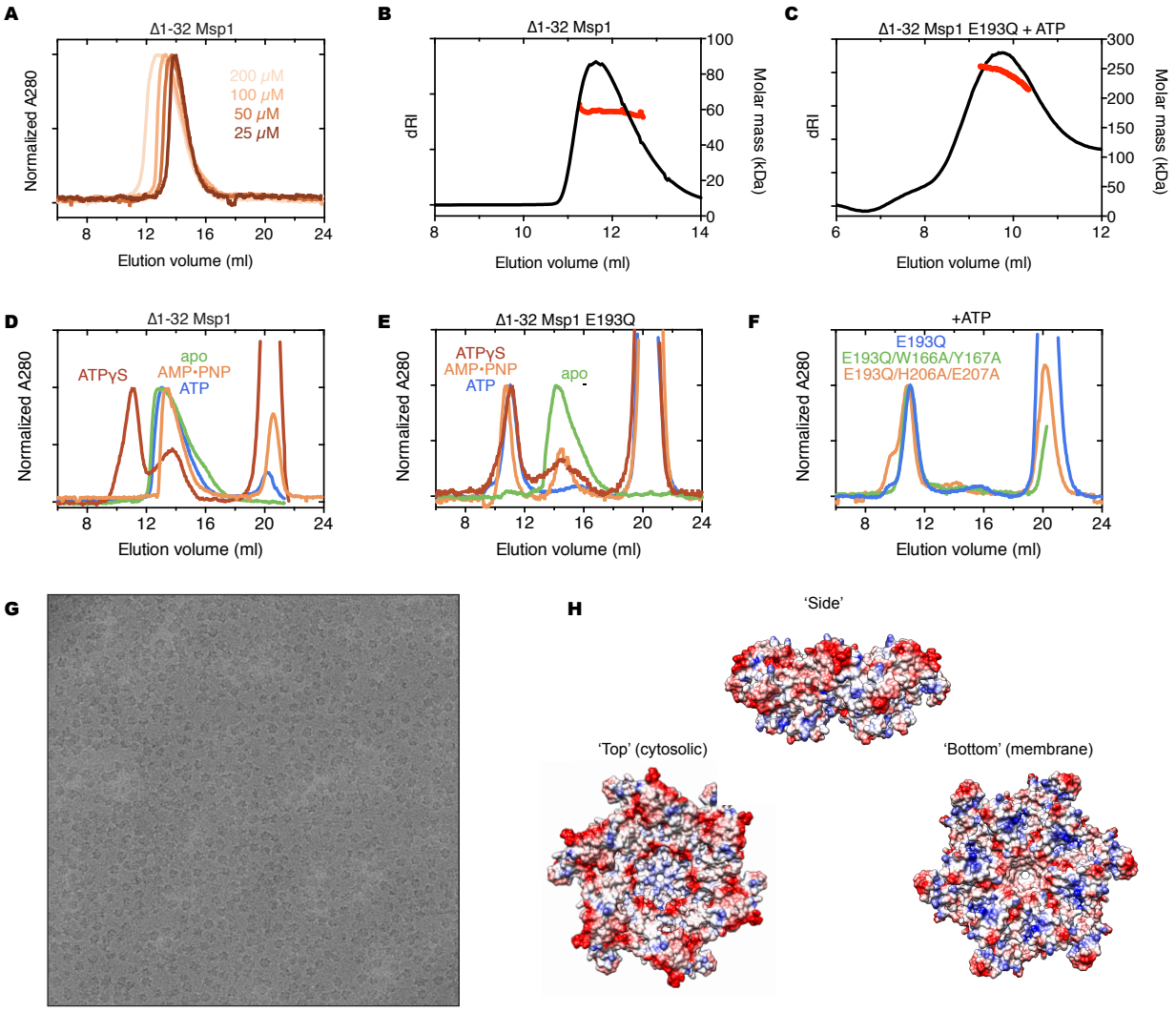

Figure S4, related to Figures 3 and 4. Additional analysis of soluble Msp1 hexamers. (A) SEC traces for the soluble region of Msp1 (Δ1-32) reveal a concentration-dependent shift towards a dimeric species in the absence of nucleotide. (B) SEC-MALS trace of soluble Msp1 shows a mixture of monomeric and dimeric species at 250 μM; the calculated mass of monomeric, soluble Msp1 is 39.1 kDa and the observed mass is 58 kDa. (C) SEC-MALS trace of the ATPase-deficient E193Q mutant of soluble Msp1 obtained in the presence of Mg^{2+}ATP. The observed molecular mass of 241 kDa agrees with the expected mass for a hexamer (235 kDa). Note that SEC was performed on an S200 Increase column at 4° C whereas SEC-MALS was performed on an S200 column at room temperature, so the elution volumes are not directly comparable. (D) SEC traces of soluble wild-type Msp1 in the presence of different nucleotides. Hexamers are observed in the presence of ATPγS but not ATP or AMP•PNP. (E) As in D, but with the E193Q mutant of Msp1; this construct forms hexamers in the presence of ATP as well as the non-hydrolzyable analogs ATPγS and AMP•PNP. (F) Pore loop mutations introduced into the soluble E193Q construct form hexamers in the presence of ATP. Note that ATP was included in the running buffer for the pore loop 1 mutant. (G) Single-particle cryo-EM of Msp1 hexamers. Representative raw micrograph of E193Q Msp1 (Δ1-32) particles in the presence of Mg^{2+}ATP. Hexameric particles with a diameter of ~13 nm are clearly visible in the raw image. Note that the majority of particles adopt a preferred orientation in the vitreous ice. (H) Electrostatic surface representation of the Msp1 hexamer model colored from negative (red) to positive (blue).

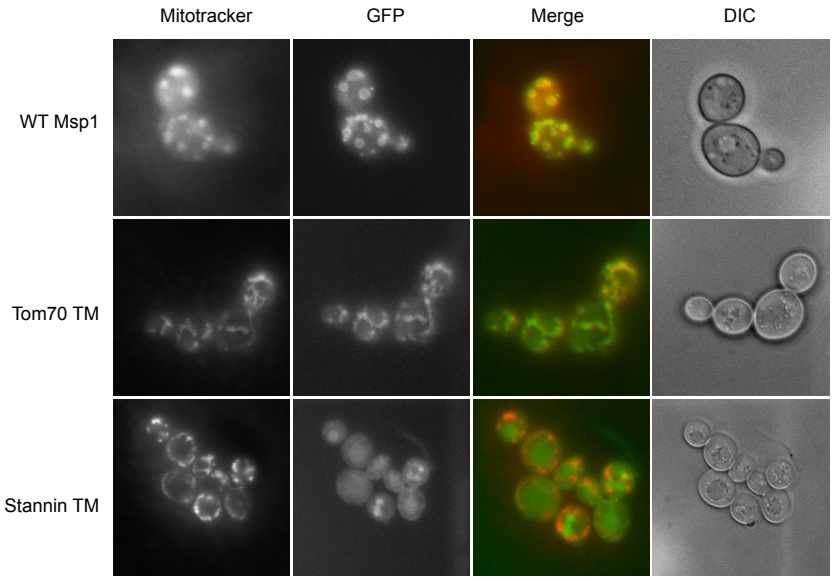

Figure S5, related to Figure 5. Localization analysis. The sub-cellular distribution of GFP-tagged Msp1 and its chimeric mutants (Tom70 TM and Stannin TM) were monitored by fluorescence microscopy in live cells. Wild-type Msp1 and the Tom70 TM chimera co-localize with mitotracker, but the Stannin TM chimera does not.